Journal of Long-Term Effects of Medical Implants, 25(3): 179–200 (2015)

A Floating Thrombus Anchored at the Proximal Anastomosis of a Woven Thoracic Graft Mimicking a Genuine Aortic Dissection

Bin Li,[a,b] Bing Liu,[c] Yijun Fu,[c] Olexandr Bondarenko,[b] Alain Verdant,[d] Olivier Rochette-Drouin,[b] Jing Lin,[c] Jean-Michel Bourget,[b] Randolph Guzman,[e] Lu Wang,[c] Ze Zhang,[b] Yvan Douville,[b] Lucie Germain,[b] Zaiping Jing,[a] & Robert Guidoin,[b,*]

[a]Department of Vascular Surgery, Changhai Hospital, Second Military Medical University, Shanghai, China; [b]Department of Surgery, Laval University and Division of Regenerative Medicine CHU de Québec Research Center, Québec, Québec City, Canada; [c]Key Laboratory of Textile Science and Technology of Ministry of Education and College of Textiles, Donghua University, Shanghai, China; [d]Department of Cardiovascular Surgery, Sacré-Cœur Hospital, Montreal and Department of Surgery, Université de Montréal, Montréal, Québec City, Canada; [e]Vascular Surgery, St. Boniface General Hospital and Department of Surgery, University of Manitoba, Winnipeg, Manitoba, Canada

*Address all correspondence to: Robert Guidoin, Department of Surgery, Faculty of Medicine, Ferdinand-Vandry Building, Room 4873, Laval University, Québec, Canada G1V 0A6; Tel.: 1-418-656-3874; Fax: 1-418-656-3821; E-mail: robertguidoin@hotmail.com

ABSTRACT: An aortoesophageal fistula following surgery for a ruptured 6.6-cm thoracic aneurysm in a 69-year-old female was repaired using a 34-mm woven prosthetic graft. A follow-up computed tomography (CT) scan at 10 days postoperatively revealed a dissection-like picture in the region of the graft, which was treated conservatively. The patient eventually died from sepsis and multiorgan failure. At autopsy, the graft was retrieved in situ and studied by detailed gross, microscopy, and scanning electron microscopy (SEM) examination. Gross observation confirmed that the dissection resulted from the rolling of the internal capsule downstream. A massive thrombus anchored at the proximal anastomosis and held by a narrow head was also noted. The thrombus demonstrated reorganization in the area of the anastomosis, with a false lumen in its distal half. The reminder of the thrombus consisted of layered fibrin. After gross examination, the fabric graft was found to be flawless. Additional detailed studies were also done using microscopy, SEM, and gross examination.

KEY WORDS: thoracic aortic graft, false lumen, floating thrombus, CT angiography, woven graft

I. INTRODUCTION

Woven vascular grafts are generally preferred for open surgery of the thoracic aorta,[1–3] based on their outstanding durability[4] and high resistance to dilatation when compared to knitted grafts.[5,6] This tight structure and the addition of albumin,[7] collagen, or gelatin[8,9] coating guarantee the imperviousness of the fabric wall at implantation. This coating begins to be resorbed in ~1 week, and a thin thrombotic matrix encroaches into the fabric and penetrates the voids in the structure to generate a bioartificial blood conduit.[10,11] The fabric behaves as a scaffold for a blood-compatible conduit, and the graft wall becomes sandwiched between internal and external capsules. Ideally, the entire flow surface would be endothelialized and synthesize prostacyclin PGI_2[12] and nitric oxide,[13] which would provide suppression of platelet activation with optimization of a low thrombotic interface. Unfortunately, this ideal of complete endothelialization of prosthetic graft surfaces does not occur in human. Biointegration and/or complete healing of an implanted graft is exposed to consecutive and competitive phenomenons qualified by Noishiki et al. as a vicious cycle with alternate sequences of healing, thrombosis, and fibrinolysis.[14] However, stenosis or thrombosis remains a very uncommon scenario in the region of thoracic aortic grafts because of the combination of a large-diameter graft associated with the shear stress caused by high blood velocity in the thoracic aorta. The formation of a floating thrombus in a native thoracic aorta represents a rare adverse event and warrants further detailed investigation.[15] The medical literature mostly highlights case reports or limited series of patients: the massive thrombus can

be anchored in the aortic arch[16–19] and descending aorta.[20–22] This pathology may be life threatening, with a significant risk of major embolism,[23,24] and aggressive treatment should be considered following the diagnosis.[25–27] Treatments can be medical with antithrombotic and/or fibrinolytic treatment[28–30] or surgical, which can be performed with thrombus removal at open surgery[31,32] or with minimal invasion (deployment of a stent-graft).[33–35] In this review, we report a unique case of a floating thrombus anchored to the proximal anastomosis of a descending aorta prosthesis by a narrow 1-cm head. The internal capsule was rolled over and a lumen stayed open in this distal segment. We present a detailed analysis of the explant in an attempt to better understand such a complex adverse event.

II. MATERIAL AND METHODS

A. Patient History Including CT Angiography

The patient, a 69-year-old woman, had conventional open repair of a ruptured aneurysm in the descending thoracic aorta. The 6.6-cm-diameter aneurysm with its surrounding hematoma had displaced the left atrium and the esophagus. Soon after the operation, she developed a septic condition with an elevated white cell count (35,000) considered to be related to either pneumonia or to urinary tract infection. A computed tomography (CT) scan done postoperatively that demonstrated the presence of air surrounding the site of repair was considered to be normal, based on open repair undertaken <30 days previously. The amount of air decreased on follow-up CTs. Five weeks later, the patient came back in profound shock with a massive upper gastrointestinal (GI) bleed and an increased amount of air around the graft (Figures 1 and 2). An aortoesophageal fistula was suspected, and an emergency prosthetic graft in situ replacement and primary esophageal repair were performed. Ten days later, a new CT angiogram disclosed a puzzling dissection-like image involving the middle body of the thoracic woven graft without involvement of the native aorta. This was treated conservatively. Unfortunately, the patient eventually died of multiple organ failure, secondary to uncontrolled sepsis. At autopsy, precise in situ retrieval of the native thoracic aorta including the Dacron graft was undertaken and conserved in formalin for further detailed investigation.

B. Biological Investigations

1. Gross Observations

The 34-mm platinum Hemashield woven double velour (HWDV) graft (Maquet, Getinge Group, Göte-

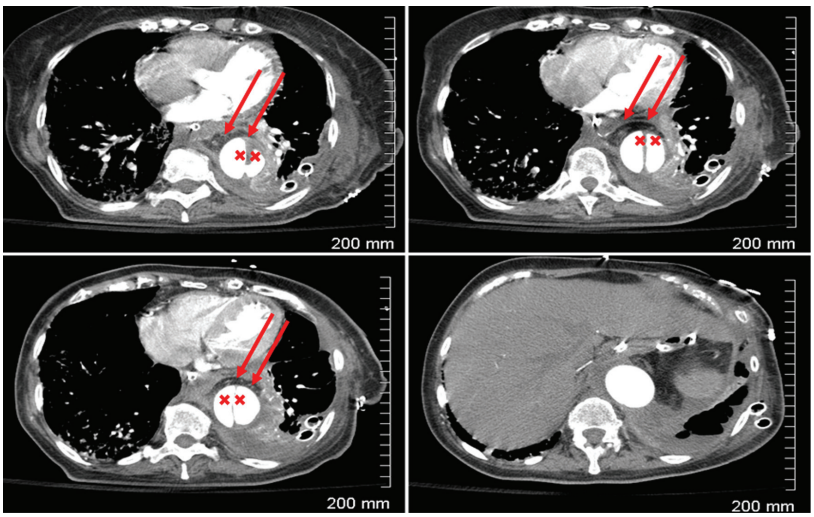

FIG. 1: CT angiogram of the thoracic aorta. Air infiltration around the prosthesis *(arrows)* indicates a possible infective process and the dissection-like image involves the middle body of the thoracic woven graft *(××)*.

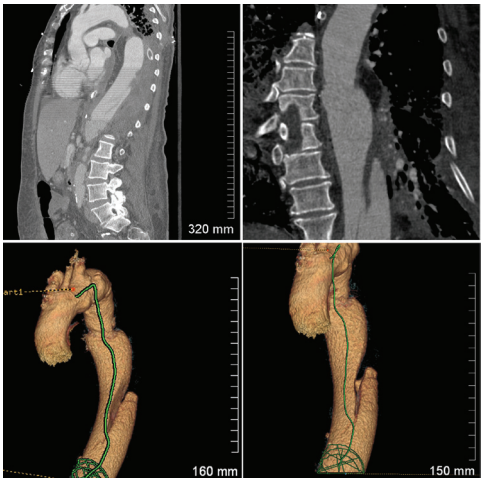

FIG. 2: CT angiogram shows reconstruction of a vascular graft implanted in the thoracic aorta illustrating the false lumen within the internal capsule.

borg, Sweden) was harvested at autopsy. It was longitudinally opened and photographed using a digital camera (Nikon, Melville, NY) (Figure 3). The flow surface was analyzed in terms of internal capsule, thrombotic deposits, and thrombus free surface, before and after fixation in a buffered solution of formalin (Figure 4).

2. Histology

Specimens 0.5 × 0.5cm^2 were selected for the histology at both proximal and distal anastomoses, in the area of diversion of the blood flow through the internal capsule, at this adhesive internal capsule, and at two sites at which the fabric structure was visible. Each specimen was divided into two subspecimens for light microscopy and scanning electron microscopy (SEM), respectively. The remaining fabric was kept for material investigation.

a. Light Microscopy

The first subspecimen was embedded in paraffin and sectioned with 5-µm thickness followed by hematoxylin/eosin staining, Weigert's resorcin-fuchsin stain to detect elastic fibers, and Masson's trichrome technique to evaluate distribution of fibrous tissue.

b. SEM

The second subspecimen was postfixed in a 2% solution of isotonic buffered glutaraldehyde and then transferred in a 1% osmium tetroxyde solution. It was dried by immersions in solutions of ethanol of grad-

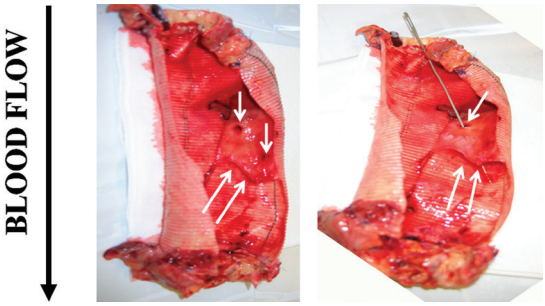

FIG. 3: Woven thoracic graft at explantation with the recanalized internal capsule. *(Needle)* Sites of entrance and escape of blood through the false lumen as observed in the distal half of the mural thrombus.

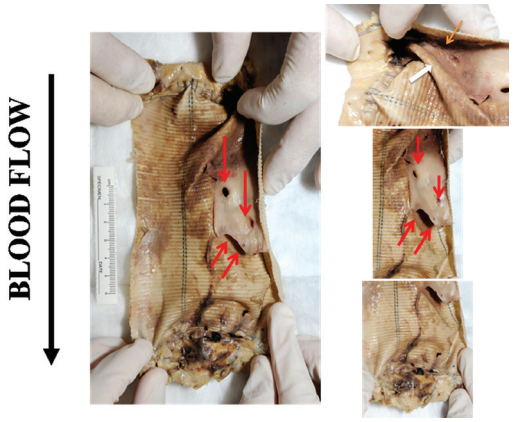

FIG. 4: Explanted thoracic graft with the recanalized floating thrombus attached by a narrow head to the site of the anastomosis. The structure of the proximal thrombus corresponds to the detachment of the internal capsule that was rolled over downstream *(white and orange arrows)*. The distal thrombus is recanalized. The false lumen shows an entrance site 5 to 6 cm from the anastomosis *(two single red arrows, left)* and one hole 4 cm downstream that permit blood to escape *(double red arrows, left)*.

ed concentrations and then in hexamethyldisilazane (Polysciences, Inc., Montreal, Canada). Further to gold palladium coating, the specimen was observed in a JEOL JSM 5600LV scanning electron microscope (Japan Electron Optics Laboratory, Tokyo) under accelerating voltages ranging from 15 to 30 kV.

C. Material Investigations

3. *Preparation of Specimens*

The explanted graft (E) and control graft (C), both HWDV prostheses 34 mm in diameter, were investigated. C was 30 cm long. One-third of C (10 cm) was kept aside and two-thirds (20 cm) were kept for examination. Tissue from E and coating from C were eliminated as follows: 5 minutes boiling in a 5% solution of sodium bicarbonate ($NaHCO_3$) and then left to return to room temperature (RT) overnight. After double rinsing in distilled water, the specimens were exposed to a 7% solution of sodium hypochlorite (NaOCl) for 30 minutes at RT. Following immersion in a 3% solution of hydrogen peroxide (H_2O_2) and shaking for 48 hours at RT, the specimens were rinsed three times in distilled water and air-dried. Each specimen was observed in a light microscope under 10× magnification to confirm the complete elimination of tissue and/or collagen coating.

4. *Gross Observations*

Guidelines for tubular vascular prostheses from the International Organization for Standardization (ISO) were followed.[36] These guidelines can be adapted for any commercially available device.[37,38]

a. *Internal Diameter in a Relaxed State*

The internal diameter was measured by a conical stem whose diameters range from 2 to 40 mm, with 0.5-mm increments. The stem was inserted into the graft until it was in intimate contact with the graft. Each assay was repeated five times.

b. *Crimping*

The creases or folds created during manufacturing to permit stretching and prevent kinking were analyzed according to the following characteristics:

- Crimp type. Naked-eyed observation was used to differentiate helicoidal crimping vs. concentric crimping.
- Crimp density. This was defined as the amount of crimp per centimeter. The tube graft was kept in a horizontal position without any pressure and stretching.
- Crimp angle. Defined as the angle between crimp and horizontal plane.

- Crimp depth. Defined as the vertical length (in millimeters) between the top and bottom of crimp.

c. Thickness

A Kawabata KES-G5 system (Kato Tech Co., Ltd., Kyoto, Japan) was used for measuring at various applied pressures. Results were extrapolated to obtain the thickness under 10 gf/cm^2 according to ISO 7198.[36]

d. Mass

Mass was obtained with an Fa2004 electronic analytical balance (to the nearest 0.1 mg) (Shanghai Wanning Precise Scientific Instrument Co., Ltd., Shanghai, China) to measure weight per unit area (g/cm^2) of the textile fabric.

e. Porosity

The percentage of void space (P) within the boundaries of the solid material compared to its total volume was calculated according to $P = 100\ (1\text{-}M/h\ \rho)$, where M represents the thickness (h, cm) of prosthetic wall and ρ the density (1.38g/cm^3) of polyester fibers.

f. Percentage of Collagen

The percentage of the mass of collagen coating within the total mass of the graft was calculated according to the following equation:

$$d(dtex) = \frac{n\rho\pi}{100} \times (\frac{D}{2})^2$$

where g represents percentage of collagen (%), m_0 the mass of the collagen-coated sample (g/cm^2), and m the mass of the cleaned sample after digestion of collagen (g/cm^2).

5. Surface Observations

a. Light Microscopy

The specimens were observed using a PXS8-T optical compound microscope (Shanghai Cewei Photoelectric Technology Co. Ltd., Shanghai, China) with a charge-coupled device (CCD) (Nikon Digital Sight [DS.Fi1], Nikon [China] Imaging Sales Co. Ltd., Shanghai), fitted with an eyepiece scale at a magnification of 40×.

b. SEM

Samples measuring 0.5 × 0.5 cm^2 were selected for examination of fabric. Particular attention was paid to detecting any damage and/or shifting of the textile yarns. In addition to the use of platinum sputtering, the samples were examined in a Jeol JSM-5600LV environmental scanning electron microscope at 15-kV accelerating voltage.

6. Yarn and Filament Analyses

a. Fabric Count

The explanted sample was compared to the control using a PXS8-T (40×) with a DS.Fi1 CCD to quantify the number of ends and picks. This permitted quantification of changes in fabric structure or distortion during implantation.

b. Number of Filaments in Each Yarn

Ten yarns were obtained at 10 different random sites in the fabric. The number of filaments was separately counted in each end and in each pick.

c. Linear Density

Mass per unit of length was calculated in decitex (decigrams per kilometer) as nominal linear density:

$$d(dtex) = \frac{n\rho\pi}{100} \times (\frac{D}{2})^2$$

where d represents the yarn linear density *(dtex)*, n the number of filaments in each yarn, ρ the density of polyester fibers (1.38 g/cm^3), and D the average filament diameter (μm).

d. Filament Mechanical Properties

Individual filaments were removed from the fabric to measure filament tensile breakage force, strength,

tensile elongation, and modulus of elasticity. These tests were conducted with an LLY-06E electronic tensile strength tester in a conditioned room with a temperature of 20°C and humidity of 65%. Gauge length was 20 mm and tensile speed was 20 mm/min. The pretension was 0.75 cN/tex. Twenty filaments for each specimen were tested and results were averaged.

7. Biomechanical Properties

a. Bursting Strength

Bursting strength was measured using a YG(B)026H (Darong Textile Instrument Co., Wenzhou, Zhejiang, China) electronic multifunction medical textiles tensile strength tester.[39] Specimens were cut into 2.5 × 2.5 cm^2 samples and loaded into the compression cage. For specimens still crimped, the crimps caused distorsions in fabric structure. The probe and jaw of the compression cage were both concentric. The probe, lowered until it just touched the test sample, traversed through the sample at a constant rate until the sample burst. Maximum bursting load was recorded for each sample. Probe burst strength was expressed in newtons. Each test was repeated three times for each sample and results were averaged.

b. Water Permeability

Water permeability was defined as the volume of cleaned, filtered water that passed during a specified period through a unit area of the wall of the graft under a specified pressure. A textile prosthesis water permeability testing device designed by Donghua University was used to test water permeability.[40] Specimens were cut into 2.2 × 2.2 cm^2 samples, submerged in cleaned filtered water at RT to wet the fabric before testing, loaded into the holder, and sufficiently stretched without distortion. Water flow was adjusted until a pressure of 16.0 kPa ± 0.3 kPa (120 mmHg ± 2 mmHg) was obtained. Flow rate of water passing through the sample for a period of 60s ± 1s was measured while the system operated under steady flow conditions. Water permeability, expressed in milliliters per square centimeter per minute (mL/cm^2/min), was calculated and recorded as follows:

$$W = \frac{Q}{A},$$

where W represents the water permeability (mL/cm^2/min), Q the flow rate through the sample (mL/min), and A the cross-section area of the aperture in the sample holder (cm^2).

8. Chemical Analysis

a. FTIR Spectroscopy

The surface chemistry of the prostheses was examined by means of a Fourier-transform infrared (FTIR) Raman spectrophotometer, model NEXUS 670 (Thermo Fisher Scientific Inc., Waltham, MA). Specimens were flattened onto the attenuated total internal reflectance system to observe the absorption bands of the fabrics. Spectra were later analyzed with OMNIC version 6.0 software for selecting absorption bands.[41]

b. DSC

Thermal properties of the polyester fabric specimens were measured by differential scanning calorimetry (DSC) in the 204 F1 (NETZSCH Machinery and Instruments Co., Ltd., Shanghai, China). Approximately 3 to 4 mg of each specimen were cut and inserted into an aluminum pan and sealed. The pans were heated from 50°C to 300°C, with a programmed heating rate of 20°C/min. Data were collected and analyzed using Proteus thermal analysis software to calculate the premelt onset temperature, peak melting temperature, heat of fusion (area under the premelt and melt peaks), degree of crystallinity, and any other endotherms and exotherms for each specimens. T_g (glass transition temperature) was continued after the above-mentioned heating phase, and the specimens were rapidly cooled to 50°C and maintained for 15 minutes before being again heated to 300°C at the same heating rate. Data were collected and analyzed in the same manner as was used to calculate T_g.

III. RESULTS

A. Morphology

The floating thrombus, 9 cm long and holding the false lumen within its distal section, showed a 1-cm-wide head anchored to the proximal anastomosis as it originated from the suture line. This thrombus was a one-piece solid mass. No visible site of possible fragmentation was evidenced on gross observation. In the proximal section of the thrombus, it was clearly visible that the internal capsule was rolled downstream from the anatomosis because of the shear stress caused by blood flow (Figure 3). The first 5 cm were red to gray, whereas the 4 cm distally were solely gray and showed the false lumen: Blood penetrated proximally through two holes and escaped distally through a major hole. The apposition of the luminal layer to the fabric was very weak and detached from the fabric wall closer to the shrinkage of the thrombus after fixation in formalin. The two .5-cm holes permitted blood to enter through the false lumen and the hole measuring 1.5 × 0.5 cm permitted blood to exit. Some additional microthrombi were observed mainly at the anastomosis sites and along the floating thrombus in contact with the prosthetic wall. The structure of this thrombus was dense and without fragmentation evident by eye-naked observation (Figure 4).

The likely sequence of events leading to this appearance was that first an internal capsule made of a thrombotic matrix in reorganization developed over the luminal surface of the fabric after the collagen was eliminated. Subsequently, part of this internal capsule became detached and rolled over downstream because of the high shear stress caused by blood flow in the thoracic aorta. This was a result of the poor penetration of this thrombotic matrix within the fabric, associated with the tight structure of the weave. The false lumen was probably the result of such a phenomenon, with the woven structure not porous enough to allow the internal capsule to become sufficiently adherent. Massive embolization did not occur because of the narrow 1-cm head of thrombus anchored to the proximal anastomosis.

The aorta at the proximal anastomosis was necrotized, holding numerous polymorphonuclear leukocytes (PNLs). The diffuse inflammatory infiltration penetrated the adventitia surrounding the vasa vasorum and the nerves. Diffuse hemorrhages were distributed in all of the layers of aortic wall. Some advanced atherosclerotic plaques were located at "intima-media" interconnections at different steps of their evolution: fatty-necrotic core with scattered inflammatory cells, huge fibrous capsule, and calcification. Crystals of cholesterol were abundant. The internal capsule showed granulation located distally at the anastomosis. Chronic inflammation was present in this area, as confirmed by the infiltration of the mononuclear cells: lymphocytes, plasma cells, macrophages, and single giant cells. Weigert's and Masson's trichrome stainings demonstrated elastolysis and development of fibrous tissues around necrotic areas and areas surrounding plaques. The mural thrombus was directly attached to the necrotized aortic wall along the anastomosis by a narrow 1-cm-wide head. The distal section of the thrombus wall was made of layers of fibrin of different age origins. The structure showed different morphologies depending on the density of the strata from granular to dense and laminated. Some fresh tiny thrombotic deposits were encrusted in the surface of the false lumen as well. The floating thrombus presented numerous sites of high fragility with fractures, leading to the formation of potentially embolizing structures (Figures 5–10).

These observations were confirmed using SEM. The proximal section of the mural thrombus was characterized by a very limited uptake of platelet and absence of red blood cells on the surface. The shear stress caused by blood flow pushed down the most fragile layers of fibrin. The flakes of older fibrin strands were more resistant to the downstream forces of blood flow. Strata of different ages were clearly identified. The thrombus was composed mainly of fibrin that was loose in texture when newly formed but progressively became more compact. This remained a condensation of fibrin, which could have been misidentified as fibrous tissue. Some structures were fragmented and were likely sources of potential embolization. Despite the appearance of a solid mass, the layers of fibrin exposed to blood flow were lifted up in several locations (Figures 11–14).

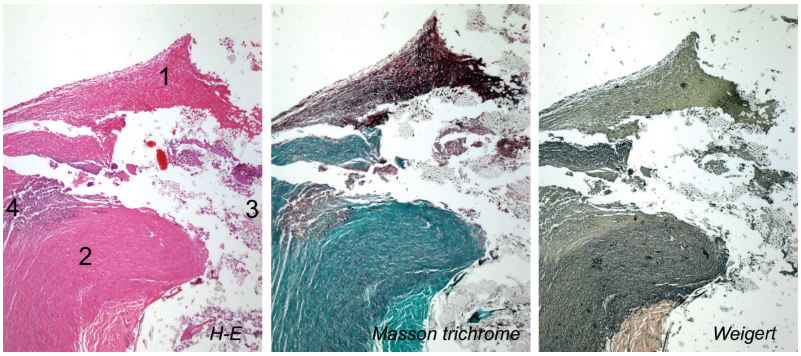

FIG. 5: General view of injury site with common pathological events. *1,* Mural thrombus; *2,* native aorta; *3,* aortic graft; *4,* leukocyte infiltration. *(Left to right) H-E,* Hematoxylin/eosin; Masson's trichrome; Weigert's elastin staining methods. (Mosaic images composed using three cascade fields of view [×40].)

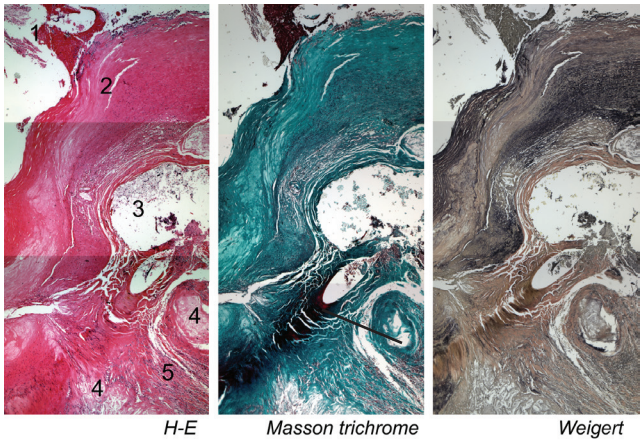

FIG. 6: Site of proximal anastomosis. *1,* Mural thrombus; *2,* native aorta; *3,* aortic graft; *4,* leukocyte infiltration; *5,* xxxxxxx. *(Left to right) H-E,* Hematoxylin/eosin; Masson's trichrome; Weigert's elastin staining methods (×40).

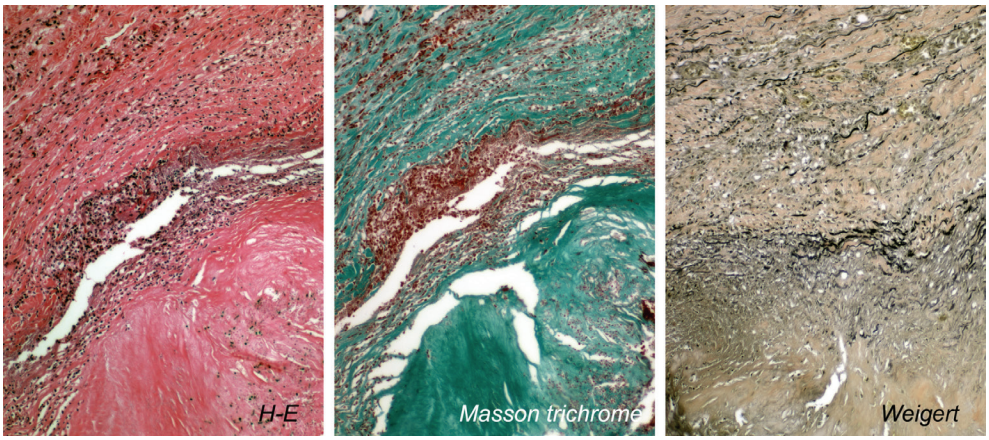

FIG. 7: Thrombus anchoring site. *1,* Thrombus head; *2,* native aorta. All panels of these pictures can be easily distinguished by Masson's trichrome *(middle panel)*: collagenous matrix of aortic wall stained *green*; fibrin masses stained *red* and *purple. (Left to right) H-E,* Hematoxylin/eosin; Masson's trichrome; Weigert's elastin staining methods (×200).

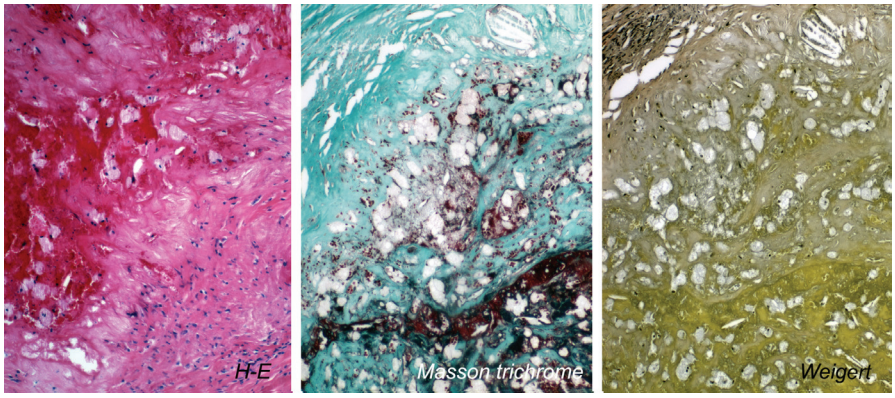

FIG. 8: Severe infiltration by PNL around fibrous atherosclerotic plaque (*bottom right* of all images). Note the remains of elastic fibers (black stained fibers in upper-left corner of right panel). *(Left to right) H-E,* Hematoxylin/eosin; Masson's trichrome; Weigert's elastin staining methods (×200).

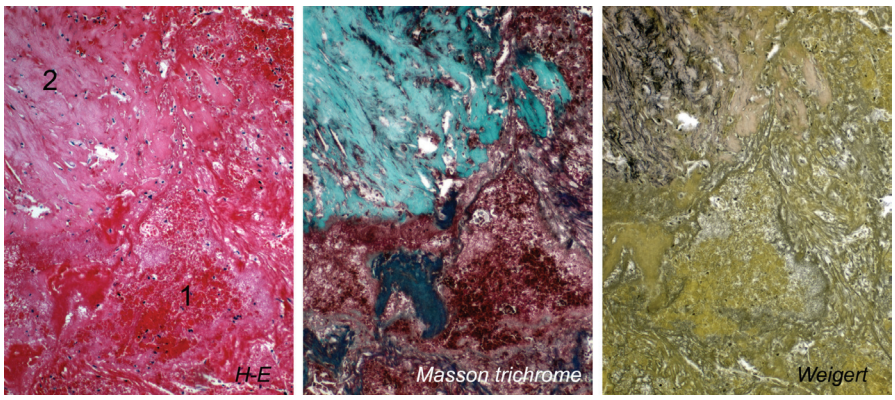

FIG. 9: Atherosclerotic plaque (atheroma) occurred at anastomosis site. Note the fibrous capsule around *(green area in middle panel)* and lipid depositions within the plaque (unstained areas in *all panels*). *(Left to right) H-E,* Hematoxylin/eosin; Masson's trichrome; Weigert's elastin staining methods (×200).

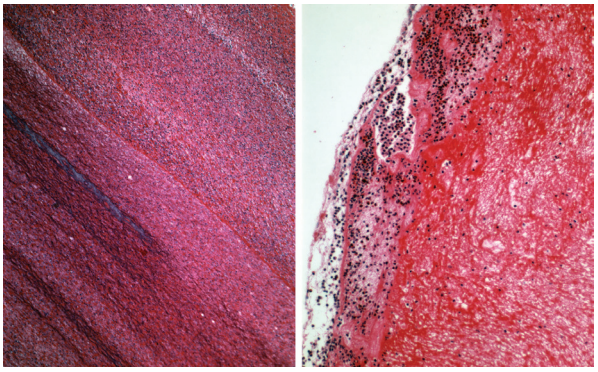

FIG. 10: Thrombus body histology. *A,* Stratification of the thrombus. Parallel layers of fibrin masses with different densities and different amounts of trapped leukocytes reveal the distinct feature of a thrombus of arterial origin (Zahn's lines). (Hematoxylin/eosin staining method [×40].) *B,* A significant amount of PNL on the thrombus surface represents the septic process diagnosed in the patient. (Hematoxylin/eosin staining method [×400)].)

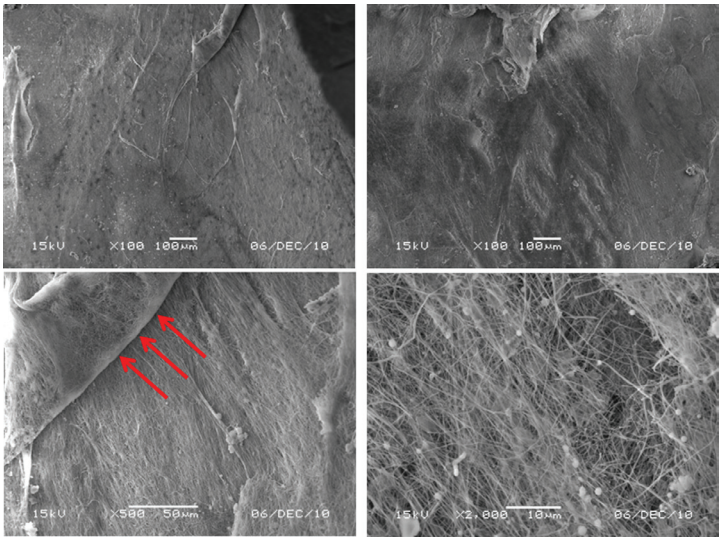

FIG. 11: SEM microphotographs taken in the vicinity of the hole entrance of blood flow through the false lumen. Internal capsule is made of consecutive layers of fibrin, which can eventually be rolled over downstream *(arrows)*.

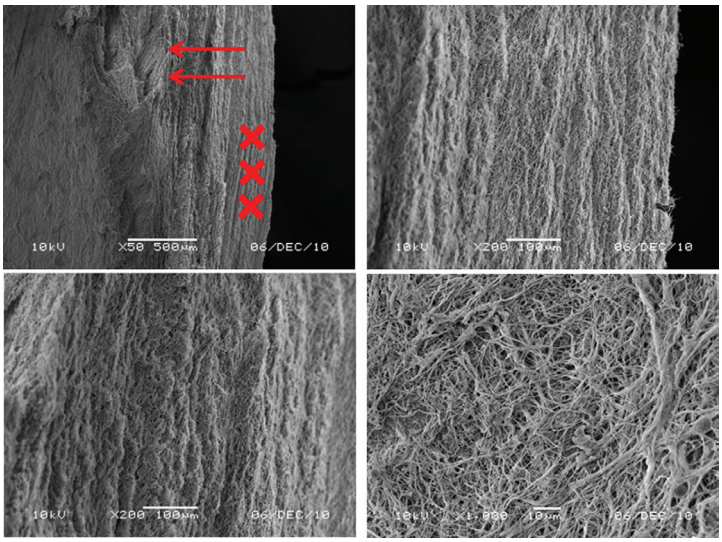

FIG. 12: Cross section of false lumen seen using SEM. Layers of fibrin show some accumulation in nodes (double red arrows) beside well-organized consecutive layers *(×××)* devoid of cell accumulation.

B. Textile Analysis

1. Gross Observations

Figure 15 provides a schematic view of the warp (parallel to the blood flow) and weft (perpendicular to the blood flow) direction to help in understanding the phenomenon of stretching and dilatation. As shown in Table 1, the relaxation diameter of the control sample (C) with and without coating was 38 mm. The concentric crimps on the C and explanted sample (E) showed a crimp density of ~6/cm, crimp angle around 60°, and crimp depth of ~0.77 mm. Thickness of C with coating was 0.55 mm; this was thicker than the samples without coating of both C and E, which were ~0.35 mm. Mass of C

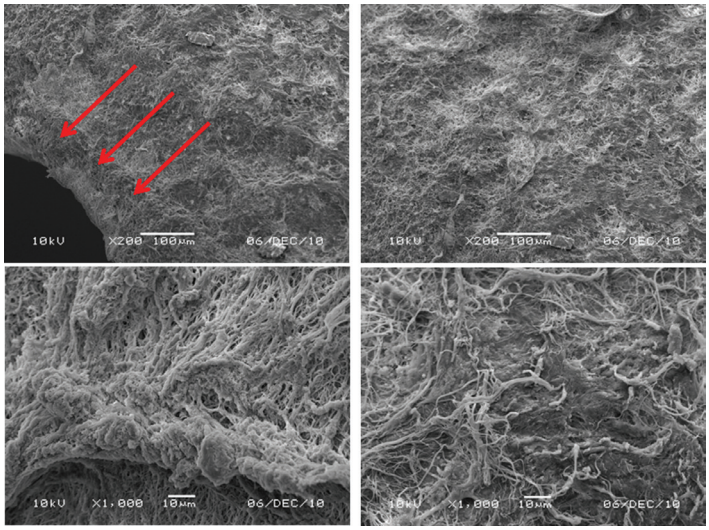

FIG. 13: Surface of the floating thrombus seen using SEM. Distal hole permits blood flow to escape through the false lumen composed of fibrin devoid of cell accumulation *(arrows)*.

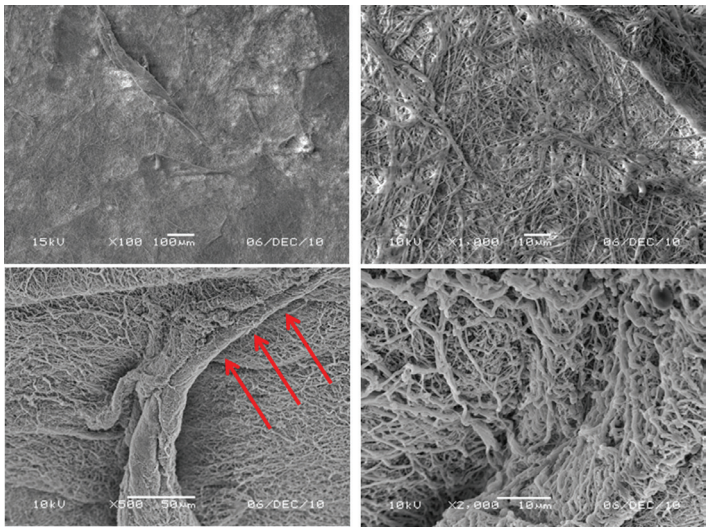

FIG. 14: Surface of the floating thrombus seen using SEM, illustrating the fragility of superficial layers of fibrin that can be moved downstream *(arrows)*.

with 42.3% coating was much higher, at 0.0395 g/cm², compared to the fabric without coating (0.0228 and 0.0184 g/cm², respectively). Porosity of E was slightly higher than C without coating. Fabric structure of both C and E were 6/4 twill and 1/1 plain.

2. *SEM*

SEM photos confirmed the crimping of fabric tubes and homogeneity of the coating (Figure 16) on the woven fabric of C. The collagen coating was regular, thin, and adequate to make the prosthetic fabric wall completely blood tight at implantation. After cleaning, the 6/4 twill and 1/1 plain fabrics were well evidenced with a regular weave (Figure 17). Yarns at the site of the bottom of the crimps showed some minor deformations in C and E, due to the crimping procedure.

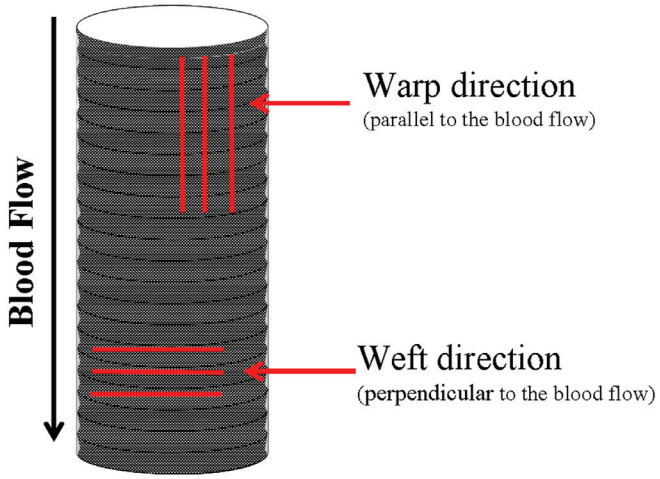

FIG. 15: Image of blood conduit, indicating warp direction (direction of blood flow) and weft direction (perpendicular to blood flow).

TABLE 1: Gross observation

Feature	Control		Explanted
	Coated sample	Cleaned sample	
Relaxation diameter (mm)	38	38	/
Crimp density (/cm)	5.60±0.09	6.22±0.04	5.31±0.03
Crimp type	Concentric	Concentric	Concentric
Crimp angle (°)	62	61	58
Crimp depth (mm)	0.77±0.01	0.78±0.02	0.67±0.05
Thickness (mm)	0.55±0.01	0.35±0.02	0.33±0.02
Mass (g/cm^2)	0.0395±0.003	0.0228±0.003	0.0184±0.008
Collagen content (%)	42.3	0	0
Porosity (%)	/	52.86	59.45
Fabric structure	6/4 twill and 1/1 plain	6/4 twill and 1/1 plain	6/4 twill and 1/1 plain

3. *Yarn and Filament Features*

Yarns in the warp direction, that is, those parallel to blood flow direction, consisted of 54 individual filaments, whereas the weft, that is, those perpendicular to the direction of blood flow, consisted of twofold yarn holding 54 filaments each. The diameter of each individual filament with roundness cross section was ~12.5 µm. The filament linear density in decitex, calculated after measuring the diameter of filament, decreased after implantation in both directions: warp went from 1.71 down to 1.42 and weft from 2.06 to 1.49. The same thread was observed in yarn linear density in decitex: a decrease after implantation from 92.1 to 76.63 in the warp and from 222.3 to 160.79 in the weft. The tensile performance of the filaments (the mean value of 10 tests) confirmed the same trend (Table 2). The tensile performance of E samples decreased compared to C samples in both warp and weft direction as a result of implantation. Filaments in the wefts showed higher tensile breakage force and tensile elongation than filaments in warps; those in the warps were permitted a better support for blood pulsation, thus guaranteeing long-term durability of the device in terms of preventing device dilatation (Figure 18).

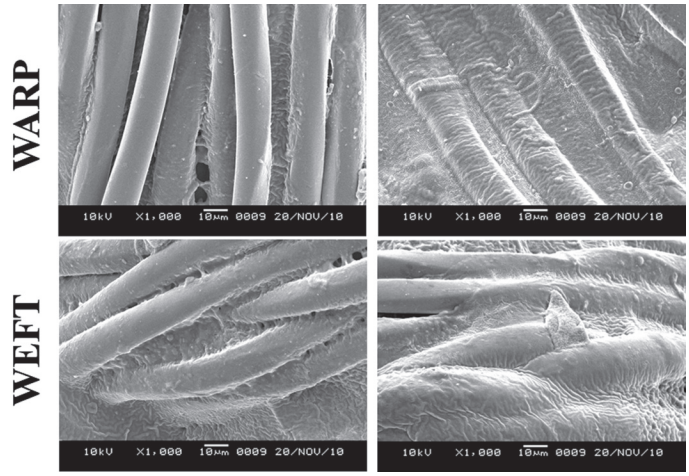

FIG. 16: SEM of control vascular graft. Collagen coating fills all interstices of yarns in both warp (parallel to blood flow) and weft (perpendicular to blood flow). Wall is thus impervious at implantation.

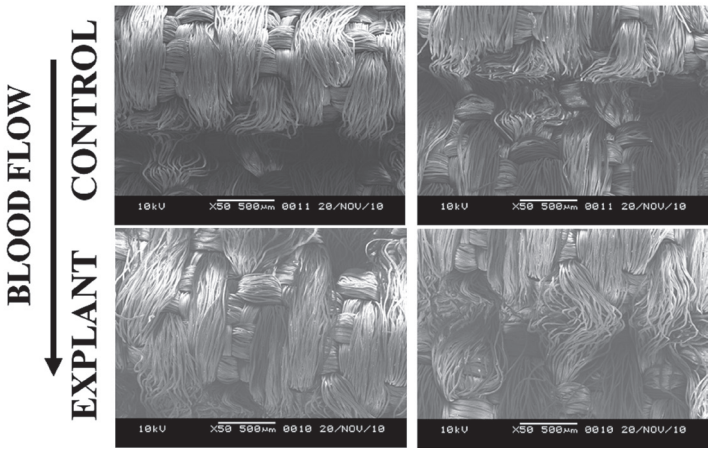

FIG. 17: SEM of cleaned control and cleaned explant. Implantation did not cause any damage to the device.

4. Probe Burst Strength

Probe burst strength of collagen-coated C was 405.34 N, higher than that of uncoated C (387.04 N). But strength decreased during implantation (demonstrated in E at 295.30 N) as a result of the fatigue of the structural modification during implantation and fluid uptakes (Table 3).

5. Water Permeability

The average value of water permeability of collagen-coated C was 3.936 mL/cm^2/min; this was almost impervious and blood tight. Water permeability values of cleaned C and E samples were similar, averaging to 230 mL, but there was great variability depending on site of the grafts (Table 3; Figure 19).

6. FTIR Analysis

FTIR spectrograms of C (before and after digestion of the collagen) and E samples after cleaning are shown in Figures 20–22. The collagen coating of the device as received from the manufacturer showed characteristic peaks at wave numbers of 3325, 2936, and 2993 cm^{-1}.The characteristic absorption spectrum of both cleaned C and E devices could be superposed, and the stretching vibration of the C=O group

TABLE 2: Yarn and filament features

Feature	Warp direction		Weft direction	
	Control	Explanted	Control	Explanted
Fabric count (/mm)	4.91±0.11	4.50±0.11	3.62±0.09	3.79±0.07
Number of filaments in each yarn	54	54	54×2	54×2
Yarn linear density (dtex)	92.1	76.63	222.3	160.79
Filament cross section	Roundness	Roundness	Roundness	Roundness
Filament diameter (μm)	12.55±0.74	11.45±0.79	13.78±0.56	11.72±0.39
Filament linear density (dtex)	1.71	1.42	2.06	1.49
Filament tensile breakage force (cN)	5.08±0.17	4.96±0.09	6.19±0.04	5.75±0.06
Filament tensile elongation (%)	53.06±0.29	54.61±0.11	75.29±0.09	67.39±0. 11
Filament tensile breakage strength (cN/dtex)	2.97±0.16	3.49±0.10	3.00±0.04	3.86±0.06
Filament modulus of elasticity (cN/dtex)	19.47±0.36	17.03±0.28	7.63±0.31	10.45±0.31

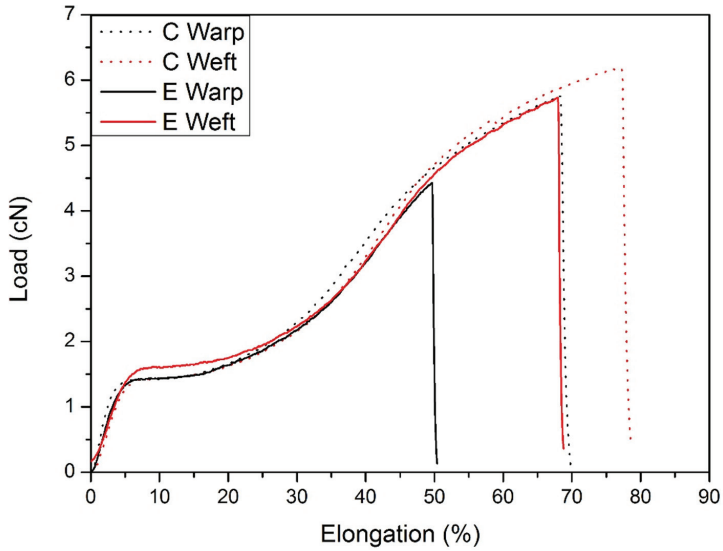

FIG. 18: Load elongation curves of the filaments in the wefts (perpendicular to blood flow) and warps (parallel to blood flow) in control (C) vs. explant (E).

TABLE 3: Biomechanical features

Feature	Control						Explanted		
	Coated sample			Cleaned sample					
Probe burst strength (N)	405.34±15.8			387.04±49.72			295.30±29.75		
Water permeability (mL/cm²/min)	No line	1 line	2 lines	No line	1 line	2 lines	No line	1 line	2 lines
	3.035±0.94	4.072±0.61	4.057±0.80	186.8±52	230.7±85	273.3±81	298.9±73	214.9±60	200.2±53
		Average			Average			Average	
		3.936±0.99			230.2±82			238±76	

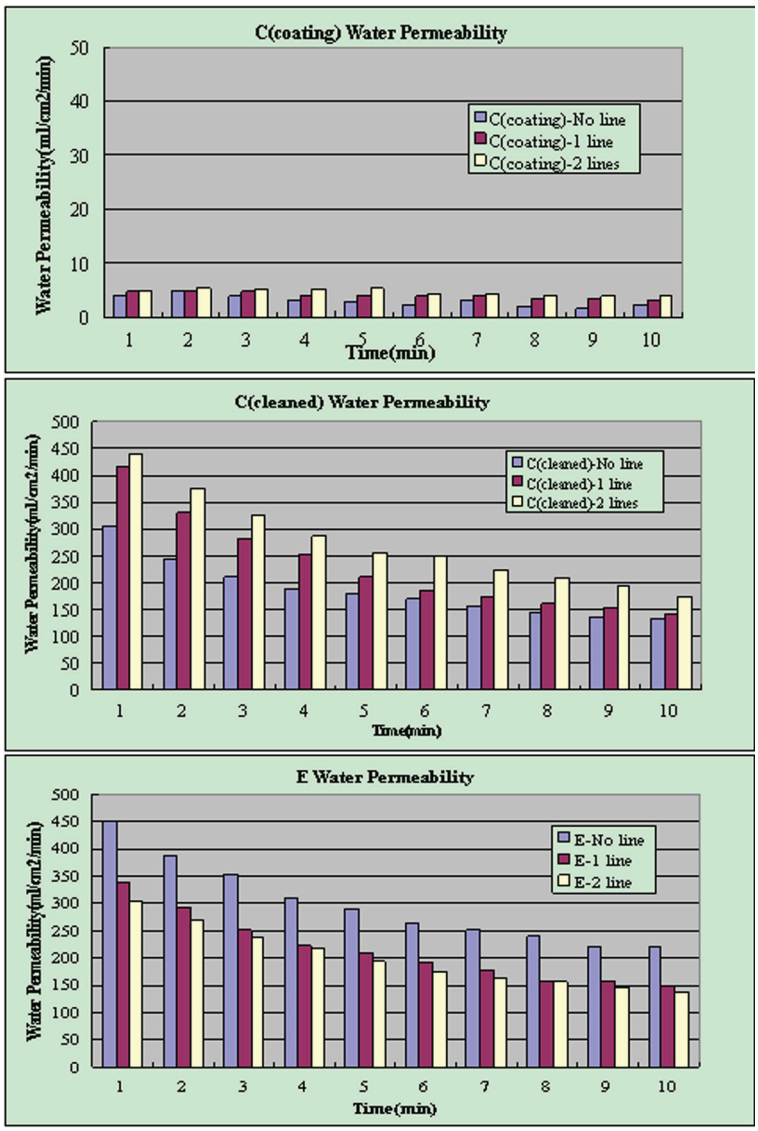

Fig. 19: Water permeability (bottom). The device as received is impervious (top) to blood at implantation, whereas after explantation, cleaning the wall of the blood conduit shows water permeability similar to the cleaned polyester fabric (middle).

at wave number 1716 cm^{-1} and that of the C–O group at 1249 and 1100cm^{-1}, along with all these characteristic absorption peaks, confirmed that the material of the graft for both C and E was the same polyester.

7. Thermal analysis

DSC testing results showed some differences between C and E. The values for heat of fusion and degree of crystallinity in E decreased moderately compared to C, indicating that implantation caused some change in the polyester fabric of the graft, a result of limited fluid and blood component uptake.

IV. DISCUSSION

When a surgeon decides to implant a medical device to treat a life-threatening pathology, complete recovery of the patient is expected.[31,32] However, significant risks to the patient exist, including complications as-

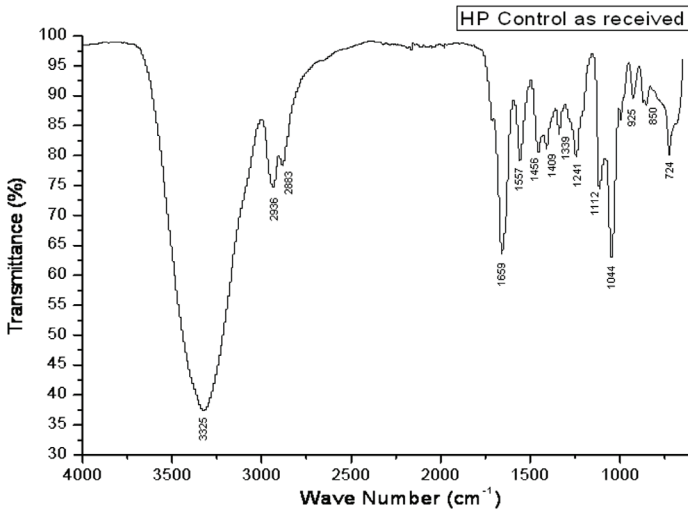

FIG. 20: FTIR spectrogram of the control prosthesis with characteristic peaks of collagen at wave numbers 3325, 2936, and 2883 cm^{-1}.

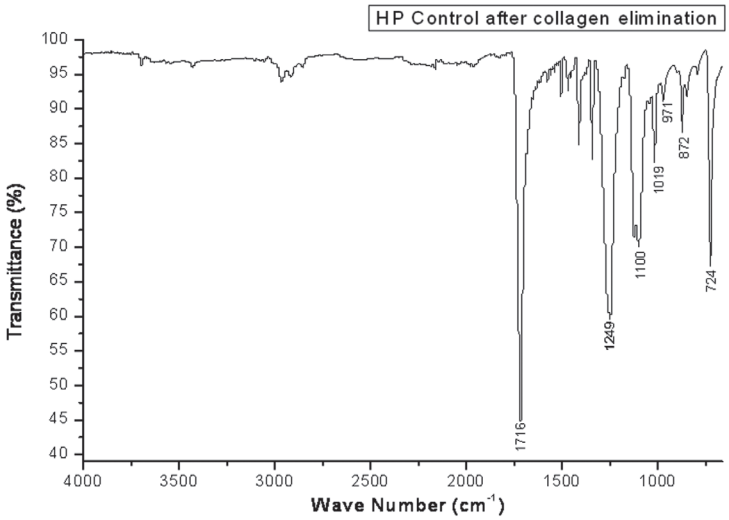

FIG. 21: FTIR spectrogram of control prosthesis after cleaning, confirming that the fabric of the graft is made of polyester.

sociated with any graft implantation. The device must restore the failing function (termed biofunctionality) and must also show a potential durability surpassing the life expectancy of the patient (biodurability). In addition, the device must become somewhat bioartificial, that is, incorporate with tissues without causing damages that the patient cannot overcome (biocompatibility). We summarize these issues as the "3Bs rule."[42] Unfortunately, adverse events can occur related to the patient, device, or surgical technique. Reporting device-related events to regulatory agencies is recommended,[43,44] because future analyses ensure further validation of implants in patients.[45]

It is worthwhile to discuss the above-mentioned case involving the 69-year-old woman, with respect to the 3Bs. The biofunctionality of the device implanted in this patient was acceptable because distal blood supply was impaired but not stopped. The issue was initially thought to be an aortic dissection but could not be considered a floating thrombus

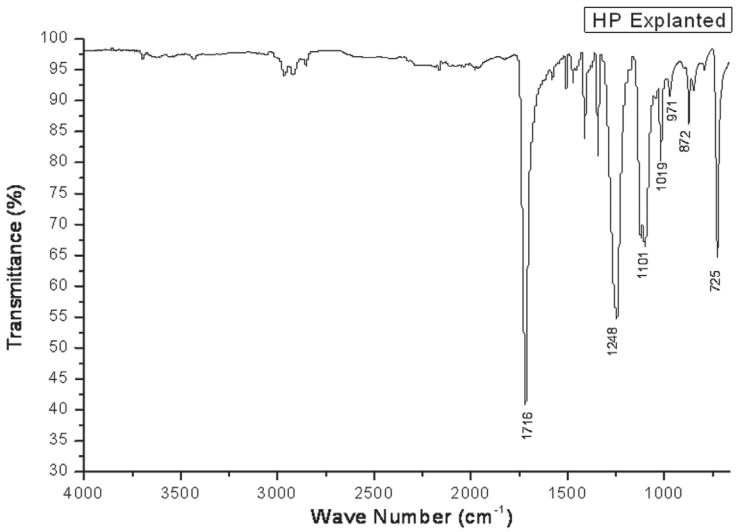

FIG. 22: FTIR spectrogram of the explanted prosthesis after cleaning. The spectrogram is superimposable to the one in Figure 21, showing that the fabric of both control and explanted devices is the same polyester.

because of weak and short attachment to the anastomosis with high risk of distal embolism. It was needless to insist that biofunctionality could have led to a high risk of distal massive embolization and that aggressive treatment was mandatory.[46] In this specific case, the thrombus was free from bacteria and therefore less likely to be fragmented in multiple emboli. However, there were some small structures that could possibly embolize and the attachment of the head at the anastomosis was narrow and weak. Such phenomena have been previously reported as case reports in the literature.[15–25] However, there were limited numbers of patients reported overall and for each report, there was no real consensus regarding the most appropriate treatment for the patient. Normally, in these cases, the objective is to eliminate and/or at least stabilize the thrombus.[35] A very aggressive medical approach with anticoagulation and/or thrombolysis is feasible, but the risk of fragmentation of the thrombus can be very high. This is supported by the observation that distal embolization may occur. A surgical thrombectomy is possible but depends on the size and location of the thrombus. An open surgical excision is very invasive but allows elimination of the thrombus and adequate reconstruction. Treatment by deploying a stent-graft using a minimally invasive approach is worth considering because there is no need for cardiopulmonary bypass. This option is currently being investigated and already recommended by opinion leaders. For example, Criado et al. advocates deployment of a stent-graft to repair a mobile thrombus.[33] And according to Fueglistaler et al., a major thrombus is a source of thromboembolism, and the stent-graft is an effective treatment compared to the systemic anticoagulation and surgical procedures that may hold comparatively higher risks.[35]

Let us now address the issue of biodurability. Polyester and Teflon are the only two polymers still implanted as blood conduits more 50 years after their introduction in vascular surgery.[47,48] Over the years, their manufacturers have improved the quality of the products and their long-term durability is well established despite anecdotal reports of failures.[49–54] Almost all devices nowadays implanted are blood tight at implantation, thanks to a bioabsorbable coating made of collagen or gelatin.[38,55,56] Structure of the fabric can be a weave or warp-knit based on their structural stability.[57] Weft-knit devices are now history because of the risk of dilatation.[58] Woven devices are given preference in the thoracic aorta because they are reportedly less prone to dilatation and thus mechanical remodeling at the anastomotic site of the aorta is not an issue. Regretfully in the literature, there is a confusion regarding the discussion of increasing diameters of fabric conduits. After im-

plantation, there is a relaxation in the structure of the fabric, inappropriately called dilatation by most of authors, including us in our early publications.[1,5,59] The real dilatation occurs after long-term implantation as the result of fatigue and is associated with fiber deterioration.[60] The phenomena hereby reported confirmed that the fabric did not show any risk of instability that can be associated with dilatation of the polyester conduit.

The last of the 3Bs is biocompatibility, an equally important issue. Assuming the histological findings, we must discriminate among what was ideally anticipated,[61,62] what is frequent,[63] and what is rare and unique.[64] Collagen coating impregnates the polyester fabric to render it blood tight during surgery; the preclotting used in the early years of vascular surgery is thus eliminated.[65,66] Any voids left by degradation of collagen are thus filled and encroach a thrombotic matrix that is reorganized. The fabric is a scaffold coated internally by the internal capsule and externally by the external capsule. This fabric scaffold is the structure that supports the development of a bioartificial blood conduit.[67–70] Thickness of the internal capsule is kept very thin, thanks to the shearing stress exerted by blood flow. The competition of fibrinolysis during healing sequences helps to prevent graft occlusion should blood velocity be greater than thrombotic threshold velocity.[71–73] The thrombotic internal surface coating is progressively discolored and the structure becomes fibrous with lacunas. Fibroblasts invade the structure and collagen is synthesized. The flow surface can be endothelialized to synthesize prostacyclin PGI_2[74] and nitric oxide.[75] This endothelialization, occurring too rarely, allows a break in the vicious cycle of thrombosis and fibrinolysis, as defined by Noishiki et al.[14] The expression of fibrinolysis activators and inhibitors is a good indication of surface thrombogenicity. With this specific device, healing sequences were burdened by the presence of atherosclerotic plaques at the anastomoses, but more specifically, at the proximal anastomosis.

Vascular surgery by itself might be considered a risk factor for thrombosis, but in this specific case, thrombogenicity was exacerbated by the presence of atherosclerotic plaques at the site of proximal anastomosis. Obviously, the head of the thrombus was anchored directly on the anastomosis, because several conditions occurred on the site to trigger the coagulation cascade: turbulence due to folds of the graft, injured atherosclerotic plaque, and severe inflammation. Most likely, surgical injury of atherosclerotic plaques led to the release of fatty-necrotic debris into surrounding tissues, which induced the inflammatory response. Necrotic tissue is a potent stimulator of inflammation that can lead to a cascade of pathological events including complementary activation, triggering of a chemokine up-regulation, and recruitment and migration of PNLs to the injury site. Although neutrophilic sequestration is targeted to neutralizing and restricting the injurious agent, the release of proteases and oxidizing agents induces additional injury to tissue, including the adjacent endothelium. This is an obvious factor of endothelial damage that is sufficient to induce blood coagulation and can be revealed histologically by the presence of significant PNL infiltration and the occurrence of injured atherosclerotic plaque at the site of anastomosis. Thrombus formation on the biomaterial surface is a commonly observed complication concerned with the coagulation of blood plasma and platelet activation. Thrombogenicity of biomaterials depends on surface chemical properties and characteristics of blood flow in which the biomaterials are involved. Biomaterial–protein interaction is the initial step of the coagulation system, in which factor XII is activated after initiation of the intrinsic coagulation pathway, ultimately followed by the production of fibrin. After the interaction between the adsorption of protein (vitronectin, fibronectin, and von Willebrand factor) and the specific receptor on the platelet membrane, the platelet is activated. The activated platelets adhere to the surface of biomaterial or aggregate. Regrettably, the woven structures cannot become a pure scaffold that permits secure encroachment and adherence to an intercommunicating capsule to become sandwiched within a composite blood conduit. The development of this 5-cm-long by 2-cm-wide capsule incorporating a false lumen represents a very unique feature.[76–88]

V. CONCLUSION

The short-term adverse event described in this case is a highly life-threatening pathology that warrants

further consideration for immediate treatment. The floating thrombus showed fissures and its head that linked the thrombus at the anastomosis site was narrow and weakly immobilized. Multiple small or massive detachment of the thrombus can result in catastrophic embolization of distal vessels. Surgical intervention, either open or minimally invasive, is the recommended treatment. Medical treatment of this particular condition with antithrombotic therapy would likely be insufficient in addressing the massive thrombus load and embolization potential. This represents a unique case of massive thrombus and significant embolization risk.

ACKNOWLEDGMENTS

This research was supported by 111 Project B07024 Biomedical Textile Materials Science from the Chinese Ministry of Education, China; the National Natural Science Fund of China (30972942) at Changhai Hospital, Shanghai, China; the International Cooperation Program supported by the Science and Technology Commission of Shanghai Municipality (10520706600), Shanghai, China; and the Department of Surgery at Laval University, Quebec City, Canada. The authors are indebted to Maquet (Jacques Blais) for the gift of the control graft. The collaboration of Marie Bolduc, Diane Lepage, Richard Janvier, Ginette Belisle, Xi Ying, Zhenyun Tang, and Yiwei Tong is greatly appreciated.

REFERENCES

1. Franke U, Jurmann MJ, Uthoff K, Köhler A, Jurmann B, Wahlers T, Borst HG. In vivo morphology of woven, collagen-sealed Dacron prostheses in the thoracic aorta. Ann Thorac Surg. 1997;64:1096-8.
2. Westaby S, Parry A, Giannopoulos N, Pillai R. Replacement of the thoracic aorta with collagen-impregnated woven Dacron grafts. Early results. J Thorac Cardiovasc Surg. 1993;106:427-33.
3. Etz CD, Homann T, Silovitz D, Bodian CA, Luehr M, Di Luozzo G, Plestis KA, Griepp RB. Vascular graft replacement of the ascending and descending aorta: Do Dacron grafts grow? Ann Thorac Surg. 2007;84:1206-12.
4. Guidoin R, King M, Blais P, Marois M, Gosselin C, Roy P, Courbier R, David M, Noël HP. A biological and structural evaluation of retrieved Dacron arterial prostheses. In: Weinstein A, Gibbons D, Brown S, Ruff W, editors. Implant retrieved material and biological analysis. Washington, D.C.: National Bureau of Standards, United States Department of Commerce. 1981;SP601:29-129.
5. Alimi Y, Juhan C, Morati N, Girard N, Cohen S. Dilation of woven and knitted aortic prosthetic grafts: CT scan evaluation. Ann Vasc Surg. 1994;8:238-42.
6. Tolan M, Wells F, Kendall S, Large S, Wallwork J. Clinical experience with collagen impregnated woven Dacron graft. J Cardiovasc Surg (Torino). 1995;36:323-7.
7. Marois Y, Chakfé N, Guidoin R, Duhamel RC, Roy R, Marois M, King MW, Douville Y. An albumin-coated polyester graft: in vivo assessment of biocompatibility and healing characteristics. Biomaterials. 1996;17:3-14.
8. Guidoin R, Marceau D, Rao TJ, King M, Merhi Y, Roy PE, Martin L, Duval M. In vitro and in vivo characterization of an impervious polyester arterial prosthesis: The gelseal triaxial graft. Biomaterials. 1987;8:433-41.
9. Bordenave L, Caix J, Basse-Cathalinat B, Baquey C, Midy D, Baste JC, Constans H. Experimental evaluation of a gelatin-coated polyester graft used as an arterial substitute. Biomaterials. 1989;10:235-42.
10. Noishiki Y. Progress and problem in the development of vascular prostheses. Art Organs. 1995;19:3-6.
11. Guidoin R, Marceau D, Couture J, Rao TJ, Merhi Y, Roy PE, DeLaFaye D. Collagen coatings as biological sealants for textile arterial prostheses. Biomaterials. 1989;10:156-65.
12. Sinzinger H, Silberbauer K, Winter M, Auerswald W. Relation between fibrinolytic activity and prostacyclin generation of atherosclerotic artery and Dacron prosthetic graft. Experientia. 1979;35:785-6.
13. Palmer RMJ, Ashton DS, Moncada S. Vascular endothelial cells synthesize nitric oxide from L-arginine. Nature. 1998:333:664-6.
14. Noishiki Y, Tomizawa Y, Yamane Y, Matsumoto A. The vicious cycle of nonhealing neointima in fabric vascular prostheses. Artif Organs. 1995;19:7-16.
15. Martens T, Van Herzeele I, Jacobs B, De Ryck F, Randon C, Vermassen F. Treatment of symptomatic mobile aortic thrombus. Acta Chir Belg. 2010;110:361-4.
16. Cañadas V, Vilacosta I, Luaces M, Bustos A, Ferreirós J, Aragoncillo P, Pérez de Isla L, Rodríguez E. Thrombosis of an apparently normal thoracic aorta and arterial embolism. Rev Esp Cardiol. 2008;61:196-200.
17. Lumia D, Carrafiello G, Laganà D, Musazzi A, Giorgianni A, Sala A, Fugazzola C. Diagnosis with ECG-gated MDCT of floating thrombus in aortic arch in a patient with type-A dissection. Vasc Health Risk Manag. 2008;4:735-9.
18. O'Sullivan J, Kerins D, Vaughan C. Massive thrombus in the aortic arch: A 59-year-old lady with an unknown familial predisposition to vascular thrombosis. Eur J Echocardiogr. 2008;9:178-80.
19. Gümüş T, Akpek S, Yücel G. Free-floating intra-aortic thrombus causing coronary artery occlusion: Appearance in ECG-gated computed tomography with cine-images. Anadolu Kardiyol Derg. 2013;13:e18-9.

20. Novacek G, Haumer M, Schima W, Müller C, Miehsler W, Polterauer P, Vogelsang H. Aortic mural thrombi in patients with inflammatory bowel disease: Report of two cases and review of the literature. Inflamm Bowel Dis. 2004;10:430-5.
21. Fontaine V, Jacob MP, Houard X, Rossignol P, Plissonnier D, Angles-Cano E, Michel JB. Involvement of the mural thrombus as a site of protease release and activation in human aortic aneurysms. Am J Pathol. 2002;161: 1701-10.
22. Mohammadi S, Trahan S, Miro S, Dagenais F. Images in cardiovascular medicine. Large free-floating intra-aortic thrombus. Circulation. 2007;116:e142-3.
23. Pousios D, Velissaris T, Duggan S, Tsang G. Floating intra-aortic thrombus presenting as distal arterial embolism. Interact Cardiovasc Thorac Surg. 2009;9:532-4.
24. Lozano P, Gomez FT, Julia M, M-Rimbau R, Garcia F. Recurrent embolism caused by floating thrombus in the thoracic aorta. Ann Vasc Surg. 1998;12:60911.
25. Choukroun EM, Labrousse LM, Madonna FP, Deville C. Mobile thrombus of the thoracic aorta: Diagnosis and treatment in 9 cases. Ann Vasc Surg. 2002;16:71422.
26. Sung HJ, Kim NH, Lim JH, Rhew JY, Yoo NJ, Oh SK, Shin SH, Lee EM, Moon Y, Choi JB, Jeony JW. Floating thrombus in the thoracic arch: A case report. Kor Circ J. 2005;35:16082.
27. Vilacosta I, San Román JA, Aragoncillo P, Ferreirós J, Mendez R, Graupner C, Batlle E, Serrano J, Pinto A, Oyonarte JM. Penetrating atherosclerotic aortic ulcer: Documentation by transesophageal echocardiography. J Am Coll Cardiol. 1998;32:83.
28. Nielsen VG, Kirklin JK, Holman WL, Steenwyk BL. Clot lifespan model analysis of the effects of warfarin on thrombus growth and fibrinolysis: role of contact protein and tissue factor initiation. ASAIO J. 2009 ;55:33-40.
29. Nielsen VG. Clot life span model analysis of clot growth and fibrinolysis in normal subjects: role of thrombin activatable fibrinolysis inhibitor. Blood Coagul Fibrinolysis. 2008;19:283-7.
30. Jacobs LA, Klopp E, Gott VL. Studies on the fibrinolytic removal of thrombus from prosthetic surfaces. Trans Am Soc Artif Intern Organs. 1968;14:63-8.
31. Achneck HE, Rizzo JA, Tranquilli M, Elefteriades JA. Safety of thoracic aortic surgery in the present era. Ann Thorac Surg. 2007;84:1180-5.
32. Westaby S, Bertoni GB. Fifty years of thoracic aortic surgery: Lessons learned and future directions. Ann Thorac Surg. 2007;83:s832-4.
33. Criado E, Wall P, Lucas P, Gasparis A, Proffit T, Ricotta J. Transesophageal echo-guided endovascular exclusion of thoracic aortic mobile thrombi. J Vasc Surg. 2004;39: 238-42.
34. Zhang WW, Abou-Zamzam AM, Hashisho M, Killeen JD, Bianchi C, Teruya TH. Staged endovascular stent grafts for concurrent mobile/ulcerated thrombi of thoracic and abdominal aorta causing recurrent spontaneous distal embolization. J Vasc Surg. 2008;47:193-6.
35. Fueglistaler P, Wolff T, Guerke L, Stierli P, Eugster T. Endovascular stent graft for symptomatic mobile thrombus of the thoracic aorta. J Vasc Surg. 2005;42:781-3.
36. International Organization for Standardization. ISO 7198. Standard for cardiovascular implants. Tubular vascular prostheses; 1998.
37. Mary C, Marois Y, King MW, Hong T, Laroche G, Douville Y, Martin L, Guidoin R. In vitro and in vivo studies of a polyester arterial prosthesis with a warp-knitted sharkskin structure. J Biomed Mater Res. 1997;35:45972.
38. Marois Y, Guidoin R, Deng X, King WM, Martin L, Roy R. The Dialine II graft: A new collagen-impregnated warp-knitted polyester arterial prosthesis. Ann Vasc Surg. 1997;11:13340.
39. Ling K. The testing instruments design and experimental research of vascular prosthesis mechanical property in vitro. MSc Dissertation, Donghua University, Shanghai, China, 2004.
40. Wang L, Jia LX. Testing device and method of water permeability of textile vascular prosthesis. Chinese Patent ZL03129179.1, 2003.
41. Thermo Nicolet Corporation. Introduction to Fourier Transform Infrared Spectrometry. http://mmrc.caltech.edu/FTIR/FTIRintro.pdf. Accessed June 11, 2010.
42. Xu Z, Fan Y, Geelkerken RM, Deng X, King M, Traoré A, Ingle N, Turgeon S, McGregor R, Dionne G, Zhang Z, Marinov GR, Legrand AP, Guzman R, Zhang H, Yin T, Douville Y, Nutley M, Renou JP, Guidoin R. Characterization of an endovascular prosthesis using the 3Bs rule (biocompatibility, biofunctionnality and biodurability): A recommended protocol to investigate a device harvested at necropsy. Long-Term Eff Med Implants. 2007;17:23762.
43. Medwatch medical reporting code instructions. Food and Drug Administration. Center for devices and radiological health. April 4, 2001. http://www.fda.gov/cdhr/mdr/373.html. Accessed September 1, 2009.
44. Medical Device Safety Reports (MDSR) 2007. Emergency Case Research Institute. Retrieved from https://www.ecri.org/default.aspx. Accessed August 17, 2009.
45. Amoore J, Ingram P. Quality improvement report: Learning from adverse incidents involving medical devices. BMJ. 2002;325:272-5.
46. Calderon P, Heredero A, Pastor A, Higueras J, Hernandez J, Karagounis PA, Aldamiz-Echevarria G. Successful removal of a floating thrombus in ascending aorta. Ann Thorac Surg. 2011;91:e67-9.
47. Couture J, Guidoin R, King M, Marois M. Textile Teflon arterial prostheses: How successful are they? Can J Surg. 1984;27:57582.
48. Chlupac J, Filova R, Bacakova L. Blood vessel replacement: 50 years of development and tissue engineering paradigms in vascular surgery. Physiol Res. 2009;58(Suppl):S119-39.

49. Pourdehimi B, Wagner D. On the correlation between the failure of vascular grafts and their structural and material properties: A critical analysis. J Biomed Mater Res. 1986;20:375409.
50. Guidoin R, Downs A, Verhaeghe JL, Roy PE, Marceau D, Fiévé G, Frisch R. Per-operative uncontrollable bleeding at polyester (Dacron) arterial prosthesis implantation. Int J Artif Organs. 1987;10:393-8.
51. Nucho RC, Gryboski WA. Aneurysms of a double velour aortic graft. Arch Surg. 1984;119:1182-4.
52. Kawamura M, Ogino H, Matsuda H, Minatoya K, Sasaki H, Kitamura S. Late-stage, nonanastomotic rupture of double-velour Dacron graft after descending aortic replacement. J Thorac Cardiovasc Surg. 2006;132:961-2.
53. Ottinger LW, Darling RC, Within LS, Linton RR. Failure of ultralightweight knitted Dacron grafts in arterial reconstruction. Arch Surg. 1976;111:1469.
54. Blumenbereg RM, Gelfand ML. Failure of knitted Dacron as an arterial prosthesis. Surgery. 1977;81:4936.
55. Quinones-Baldrich WJ, Moore W, Ziomeks S. Development of a “leak-proof” knitted Dacron vascular prosthesis. J Vasc Surg. 1986;3:895903.
56. Guidoin R, Snyder R, Martin L, Botzko K, Marois M, Awad J, King M, Domurado D, Bedros M, Gosselin C. Albumin coating of a knitted polyester arterial prosthesis: An alternative to preclotting. Ann Thorac Surg. 1984;37:45765.
57. Debille E, Guidoin R, Charara J, Torché D, Bernier-Cardou M, Marceau D, Boyer D, Chaput C, Dadgar L, Cardou A. Dilatability and stretching characteristics of polyester arterial prostheses. Evaluation of the elastic behaviour. In: Plank H, Dauner M, Renardy M, editors. Medical textiles for implantation. Berlin, Heidelberg: Springer; 1990. p. 13785.
58. Guidoin R, Gosselin C, Roy J, Gagnon D, Marois M, Noel HP, Roy P, Martin L, Awad J, Bourassa S, Rouleau C. Structural and mechanical properties of Dacron prostheses as arterial substitute. In: Hastings GW, Williams DF, editors. Mechanical properties of biomaterials. New York: John Wiley & Sons; 1980. p. 54756.
59. Guidoin R, Gosselin C, Martin L, Marois M, Laroche F, King M, Gunasekera K, Domurado D, Sigot-Luizard MF, Blais P. Polyester prostheses as substitute in the thoracic aorta of dogs. I. Evaluation of commercial prosthesis. J Biomed Mater Res. 1982;119:4439.
60. Berger K, Sauvage LR. Late fiber deterioration in Dacron arterial grafts. Ann Surg. 1981;193:47791.
61. Sauvage LR, Berger K, Beilin LB, Smith JC, Wood SJ, Mansfield PB. Presence of endothelium in an axillary-femoral graft of knitted Dacron with an external velour surface. Ann Surg. 1975;182:74953.
62. Hong-De Wu M, Shi Q, Wechezak A, Clowes AW, Gordon IL, Sauvage LR. Definitive proof of endothelialization of a Dacron arterial prosthesis in a human being. J Vasc Surg. 1995;21:8627.
63. Berger K, Sauvage LR, Rao AM, Wood SJ. Healing of arterial prostheses in man: Its incompleteness. Ann Surg. 1972;175:118-27.
64. Malyar NM, Janosi RA, Brkovic Z, Erbel R. Large mobile thrombus in non-atherosclerotic thoracic aorta as the source of peripheral arterial embolism. Thromb J. 2005;3:19.
65. Yates SG, Barros D’Sa AA, Berger K, Fernandez LG, Wood SJ, Rittenhouse EA, Davis CC, Mansfield PB, Sauvage LR. The preclotting of porous arterial prostheses. Ann Surg. 1978;188:61122.
66. Guidoin RG, Gosselin C, Rouleau C, Haggis GH, Boulay J, Awad J. Preclotting of knitted Dacron prosthesis. A scanning electron microscopy study. J Thorac Cardiovasc Surg. 1975;70:15262v
67. Merhi Y, Guidoin R, Forest JC. Fate of polyester arterial prostheses implanted as thoraco-abdominal by-passes in dogs: Haematology, pathology, and biochemistry. Clin Invest Med. 1988;11:403-16.
68. Noishiki Y, Yamane Y, Ichikawa Y, Yamazaki I, Yamamoto K, Kosuge T, Manabe T, Mo M. Age dependency of neointima formation on vascular prostheses in dogs. Artif Organs. 2000;24:718-28.
69. Grabenwöger M, Fitzal F, Sider J, Csekö C, Bergmeister H, Schima H, Husinsky W, Böck P, Wolner E. Endothelialization of biosynthetic vascular prostheses after laser perforation. Ann Thorac Surg. 1998;66:S110-4.
70. Zhang Z, Briana S, Douville Y, Zhao H, Gilbert N. Transmural communication at a subcellular level may play a critical role in the fallout based-endothelialization of Dacron vascular prostheses in canine. J Biomed Mater Res A. 2007;81:877-87.
71. Sulkin MD, Gervin AS. Fibrinolytic activity in pseudointima of Dacron aortic grafts. Am Surg. 1974;40:675-9.
72. Collen D, Stassen JM, Stump DC, Verstraete M. Synergism of thrombolytic agents in vivo. Circulation. 1986;74: 838-42.
73. Sauvage LR, Walker MW, Berger K, Robert SB, Lischko MM, Yates SG, Logan GA. Current arterial prostheses. Experimental evaluation by implantation in the carotid and circumflex coronary arteries of the dog. Arch Surg. 2979;114:68791.
74. Moncada S, Herman AG, Higgs EA, Vane JR. Differential formation of prostacyclin (PGX or PG12) by layers of the arterial wall. An explantation for the anti-thrombotic properties of vascular endothelium. Thromb Res. 1977;11:32344.
75. Palmer RMJ, Ashton DS, Moncada S. Vascular endothelial cells synthetize nitric oxide from L-arginine. Nature. 1988;333:664-6.
76. Gacko M, Głowiński S. Activities of proteases in parietal thrombus of aortic aneurysm. Clin Chim Acta. 1998;271:171-7.
77. Sprengers ED, Kluft C. Plasminogen activator inhibitors. Blood. 1987;69:381-7.
78. Kowalewski R, Zimnoch L, Wojtukiewicz MZ, Glow-

inski J, Glowinski S. Evaluation of urokinase-type plasminogen activator and its receptor in neointima of polyester vascular grafts. Pathophysiol Haemost Thromb. 2005;34:23-8.
79. Sallusto F, Mackay CR. Chemokines and their reception in hemostasis and inflammation. Curr Opin Immunol. 2004;16:724.
80. Kowalewski R, Zimnoch L, Wojtukiewicz MZ, Glowinski J, Glowinski S. Expression of fibrinolysis activators and their inhibitor in neointima of polyester vascular grafts. Biomaterials. 2004;25:5987-93.
81. Kowalewski R, Zimnoch L, Wojtukiewicz MZ, Glowinski S, Glowinski J. Coagulation activators and inhibitors in the neointima of polyester vascular grafts. Blood Coagul Fibrinolysis. 2003;14:433-9.
82. Handt S, Jerome WG, Tietze L, Hantgan RR. Plasminogen activator inhibitor-1 secretion of endothelial cells increases fibrinolytic resistance of an in vitro fibrin clot: Evidence for a key role of endothelial cells in thrombolytic resistance. Blood. 1996;87:4204-13.
83. Vogler EA, Siedlecki CA. Contact activation of blood-plasma coagulation. Biomaterials. 2009;30:1857-69.
84. Gorbet MB, Sefton MV. Biomaterial-associated thrombosis: Roles of coagulation factors, complement, platelets and leukocytes. Biomaterials. 2004:25:5681-703.
85. Jaeschke H, Smith CW. Mechanisms of neutrophil-induced parenchymal cell injury. J Leukoc Biol. 1997;61:647-53.
86. Ratnoff OD. The role of haemostatic mechanisms. Clin Haematol. 1981;10:261-81.
87. Shimazaki T, Ishimaru S, Kawaguchi S, Yokoi Y, Watanabe Y. Blood coagulation and fibrinolytic response after endovascular stent grafting of thoracic aorta. J Vasc Surg. 2003;37:1213-18.
88. Zilla P, Bezuidenhout D, Human P. Prosthetic vascular grafts: Wrong models, wrong questions and no healing. Biomaterials. 2007;28:5009-27.